IEEE Access
Multidisciplinary | Rapid Review | Open Access Journal

Received February 26, 2020, accepted March 18, 2020, date of publication March 20, 2020, date of current version April 1, 2020.

Digital Object Identifier 10.1109/ACCESS.2020.2982284

A Novel Analysis Approach for Dual-Frequency Parallel Transmission-Line Transformer With Complex Terminal Loads

TAIYANG XIE[1], XIAOLONG WANG[1], (Member, IEEE), ZHEWANG MA[2], (Member, IEEE), CHUN-PING CHEN[3], (Member, IEEE), AND GEYU LU[1]

[1]College of Electronic Science and Engineering, Jilin University, Changchun 130012, China
[2]Graduate School of Science and Engineering, Saitama University, Saitama 338-8570, Japan
[3]Department of Electrical, Electronics and Information Engineering, Kanagawa University, Yokohama 221-8686, Japan

Corresponding author: Xiaolong Wang (brucewang@jlu.edu.cn)

This work was supported in part by the National Natural Science Foundation of China under Grant 61701189, in part by the ''thirteenth five-year plan'' Science and Technology Research Foundation of Education Bureau of Jilin Province, China, under Grant JJKH20180086KJ, and in part by ''the Fundamental Research Funds for the Central Universities.''

ABSTRACT In this paper, a parallel transmission-line transformer with complex terminal loads is introduced for dual-frequency design. Through analyzing the different cases of complex terminal loads conditions, there are four different mapping patterns of designable regions on the Electrical Length-Electrical Length (*EL-EL*) plane. By adding an extra vertical Frequency Ratio (*FR*) axis, a novel 3D cube can be created on the *FR-EL-EL* coordinate system, then the designable ranges of frequency ratio can be easily drawn in this 3D cube. Therefore, the visible 3D mapping approach is newly reported for matching the complex terminal load of parallel transmission-line transformer at two different frequencies. For the certain pattern, a clearly boundary could be drawn to distinguish the designable and undesignable ranges. For verification, two examples are designed, fabricated and measured. Simulated and measured results are matched very well.

INDEX TERMS Complex terminal loads, dual-frequency, parallel transmission-line transformer, 3D mapping approach.

I. INTRODUCTION

Transmission-line transformer (TLT) is a basic passive component in RF/microwave system. For a certain frequency, it can transform a source load impedance into a different terminal load impedance and deliver the maximum power at the same time. According to the different application requirements, the input or output impedances of power transistors, antennas, power dividers, or baluns are not always real load impedance, flexible TLTs are needed to match different kinds of complex impedances.

Only one transmission-line (TL) section could not only used for real-to-real impedance matching, but also for complex-to-complex impedance matching at single-band operation [1]. Focusing on real-to-real impedance matching, by adding extra cascaded TL sections, cascaded TL sections could be designed for dual-band operation [2]–[5], or wideband performance [6]. As the number of cascaded TL sections is increased, multi-band can be realized [7]–[9]. Furthermore, multi-band cascaded TL sections could not only be designed for real impedance application, but also for complex impedance application [10]–[12].

Coupled TLT is the other basic transformer topology [13]. Compared with cascaded TLT topology, coupled TLTs could provide extra variables which can be utilized for broadband matching [13], DC blocks [14], compact circuit size [15] and multi-band application [16]. Because the designable coupling strength of coupled TLT is quite limited, shunted open-/short-stubs (OS/SS) are preferred in TLT design [17]–[21]. single-band [17], dual-band [18]–[20] or even multi-band [21] applications can be easily realized. Considering the precise bandwidth needs, several different types of band-pass filtering transformers are also reported in [22]–[26] for different system requirements. On the other hand, parallel transmission-line is another interesting structure which can be used for single-band transformer [27], filters [28], [29] and duplexer [30] applications.

Due to the limitation of the designable characteristic impedances (or electrical lengths) ranges, designable values are quite different for diverse topologies, therefore, it is a very

The associate editor coordinating the review of this manuscript and approving it for publication was Xiu Yin Zhang.

important and effective method to distinguish the circuits' performances. For example, it can be used to evaluate (1) the designable range of terminal load ratio in TLT applications, (2) the designable bandwidths of filter applications, (3) the designable range of frequency ratio in dual-frequency circuits, and so on. Comparing with the obscure constraint formulas which are derived from matching condition, allowed and forbidden regions [1], [27] could provide a quite clearly visible boundary on Smith chart, which the designable and undesignable ranges can be separated clearly. As far as we know, this method is only working on single-frequency applications. For dual-frequency or even multi-band applications, flow charts are only method to describe relationship among all mathematical constraint. Usually, several numerical examples are also listed to show tendency of all the design parameters. However, the boundary of designable range for a certain topology is unpredictable.

Recently, a dual-frequency parallel transmission-line transformer (PTLT) for real terminal loads is reported in [31], it only consists of two parallel TLs with different physical lengths. Through analyzing the physical lengths ratio, designable square regions are mapping on the *Electrical Length-Electrical Length* (*EL-EL*) plane [32], [33], and the mapping pattern of all the designable regions looks like chess board. Because [32] and [33] are only comments and authors' reply, their definitions are quite different, detail design approach and strict mathematical proof are also not clear.

In this paper, a visible 3D mapping approach is newly introduced for a dual-frequency PTLT with complex terminal loads, where the complex terminal loads at two frequencies are not independent. The 3D coordinate system consists of one *EL-EL* plane and a vertical *Frequency Ratio* (*FR*) axis named u. Usually, two electrical lengths which are on the *EL-EL* plan are defined from 0 to 2π. Through analyzing the different cases of complex terminal loads conditions, there are four different mapping patterns of designable regions on the *EL-EL* plane. When the electrical lengths ratio is given, the designable range of frequency ratio can be easily drawn in the 3D cube on the *FR-EL-EL* coordinate system. To the best of the authors' knowledge, the proposed visible 3D mapping approach has not been reported before.

For ease of understanding, a 3D mapping example for real terminal load case [31] is introduced in Fig. 1. The *EL-EL* plane has been introduced in [32] briefly, the red and blue squares are the mapping pattern of designable regions of dual-frequency PTLT, and it looks like part of chess board, where $0 < \beta_1 l_1 < 2\pi$ and $0 < \beta_1 l_2 < 2\pi$ are defined on the *EL-EL* plane. The definition of vertical *FR* axis is u, where $0 < u < 10$. For a given electrical lengths ratio, such as $\beta_1 l_2/\beta_1 l_1 = 5$ in Table 1 [33], where $\beta_1 l_1 = 56.25°$ and $\beta_1 l_2 = 281.25°$. Then, the *ABIJ* plane shows the case of $\beta_1 l_2/\beta_1 l_1 = 5$. Two solid black lines in line *AJ* are the designable ranges in the two red regions. From the design equations in [31], [32], the designable ranges u can be easily calculated and drawn as the green solid lines on the *ABIJ* plane. On the other hands, the relationship between $\beta_1 l_1$ and u (or, the relationship between $\beta_1 l_2$ and u) can also be easily calculated and drawn on *ABFE* plane (or *ABCD* plane), where $1.5 < u < 7/3$ and $4 < u < 9$.

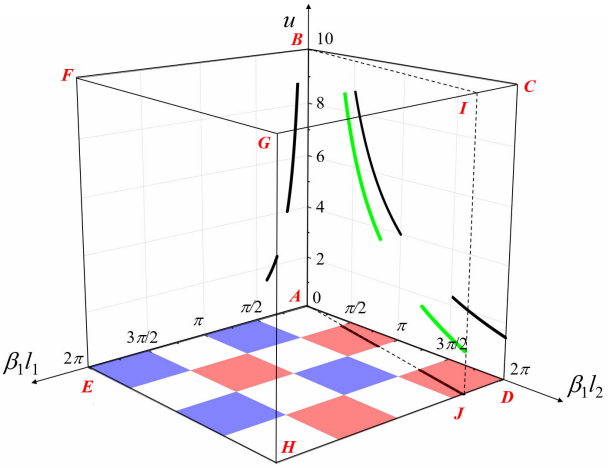

FIGURE 1. An example of visible 3D mapping approach on the *FR-EL-EL* coordinate system for dual-frequency PTLT application [31], [32].

TABLE 1. Comparison among the proposed transformer and others.

Ref.	Circuit Structure		Type of Transformer/Number of Passband	Type of Source/ Terminal Loads
	Type	Number of TLs, Coupled TLs and OS/SS		
[1]	Cascaded	1 TLs	BPT/1	Complex/ Complex
[2]	Cascaded	2 TLs	2	Real/ Real
[3]	Cascaded	2 TLs	2	Real/ Real
[4]	Cascaded	2 TLs	2	Real/ Real
[5]	Cascaded	2 TLs	2	Real/ Real
[6]	Cascaded	2 TLs	1	Real/ Real
[7]	Cascaded	3 TLs	3	Real/ Real
[8]	Cascaded	10 TLs	5	Real/ Real
[9]	Cascaded	14 TLs	5	Real/ Real
[10]	Cascaded	2 TLs	2	Complex/ Complex
[11]	Cascaded	3 TLs	2	Complex/ Real
[12]	Cascaded	4 TLs	2	Complex/ Complex
This work	**Parallel**	**2 TLs**	**2**	**Complex/ Real**

In summary, the novelty of the proposed dual-frequency PTLT with complex terminal load can be summarized as follows: (1) Novel four mapping patterns of designable regions are derived and summarized on *EL-EL* plane under the condition of different case of complex terminal loads. (2) By adding an extra vertical *FR* axis, a novel 3D cube is newly introduced on *FR-EL-EL* coordinate system for dual-frequency design application. (3) When the electrical lengths ratio is determined, the novel 3D mapping approach is reported to derive the designable frequency ratio range in the 3D cube.

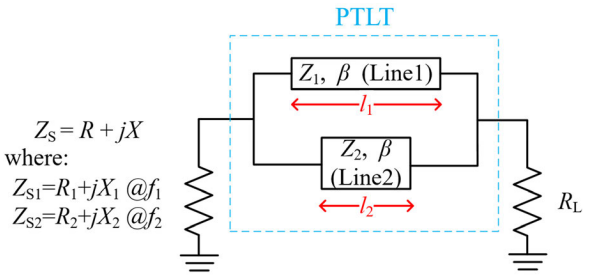

FIGURE 2. Dual-frequency parallel transmission-line transformer (PTLT) [31], [32] with complex terminal loads.

II. DESIGN EQUATIONS

Fig. 2 shows the proposed topology of the dual-frequency PTLT. Although the same topology has been introduced in [31]–[33] for real terminal loads applications, to the best of authors' knowledge, the dual-frequency analysis of 3D mapping approach is newly reported for complex terminal loads application in this paper. In Fig. 2, Z_1 and Z_2 are characteristic impedances of line 1 and line 2, respectively, and their physical lengths are l_1 and l_2, where $l_1 > l_2$ is defined in this paper. β denotes a propagation constant of the TLs. For dual-frequency operation, two design frequencies are defined as f_1 and f_2, where $f_1 < f_2$, and frequency ratio $u = f_2/f_1$. Then, β_1 and β_2 are the propagation constants at f_1 and f_2, respectively. Finally, two complex terminal loads can be written as $Z_S = R + jX$, where $Z_{S1} = R_1 + jX_1$ at f_1 and $Z_{S2} = R_2 + jX_2$ at f_2, respectively. In this paper, the terminal load $Z_L = 50\ \Omega$ is defined.

A. THE DERIVATION BETWEEN CHARACTERISTIC IMPEDANCES AND ELECTRICAL LENGTHS

From [31], *ABCD* matrices of line 1 and line 2 are expressed as

$$\begin{bmatrix} A_1 & B_1 \\ C_1 & D_1 \end{bmatrix}_{Line1} = \begin{bmatrix} \cos(\beta l_1) & jZ_1 \sin(\beta l_1) \\ j\sin(\beta l_1)/Z_1 & \cos(\beta l_1) \end{bmatrix} \quad (1a)$$

$$\begin{bmatrix} A_2 & B_2 \\ C_2 & D_2 \end{bmatrix}_{Line2} = \begin{bmatrix} \cos(\beta l_2) & jZ_2 \sin(\beta l_2) \\ j\sin(\beta l_2)/Z_2 & \cos(\beta l_2) \end{bmatrix}. \quad (1b)$$

Then, the *ABCD* matrix of proposed PTLT can be obtained in (2), since the same derivation processes are described in [31].

$$A_{PTLT} = (A_1B_2 + A_2B_1)/(B_1 + B_2) \quad (2a)$$

$$B_{PTLT} = B_1B_2/(B_1 + B_2) \quad (2b)$$

$$C_{PTLT} = (C_1 + C_2) + (A_1 - A_2)(D_2 - D_1)/(B_1 + B_2) \quad (2c)$$

$$D_{PTLT} = (B_2D_1 + B_1D_2)/(B_1 + B_2) \quad (2d)$$

In order to match the terminal load R_L, we have

$$\bar{Z}_S = R - jX = \frac{R_L A_{PTLT} + B_{PTLT}}{R_L C_{PTLT} + D_{PTLT}} \quad (3)$$

The real and imaginary parts of (3) can be derived as Real part:

$$D_{PTLT}R = A_{PTLT}R_L + jC_{PTLT}R_LX \quad (4a)$$

Imaginary part:

$$B_{PTLT} = C_{PTLT}R \cdot R_L - jD_{PTLT}X \quad (4b)$$

From $A_{PTLT} = D_{PTLT}$ and $A_{PTLT}D_{PTLT} - B_{PTLT}C_{PTLT} = 1$, the following equations can be derived.

$$\begin{cases} A_{PTLT} = G_A(R, X, R_L) \\ B_{PTLT} = G_B(R, X, R_L) \\ C_{PTLT} = G_C(R, X, R_L) \\ D_{PTLT} = G_D(R, X, R_L) \end{cases} \quad (5)$$

On the other hand, from (1) and (2), (6) can be easily derived.

$$\begin{cases} A_{PTLT} = F_A(Z_1, Z_2, \beta l_1, \beta l_2) \\ B_{PTLT} = F_B(Z_1, Z_2, \beta l_1, \beta l_2) \\ C_{PTLT} = F_C(Z_1, Z_2, \beta l_1, \beta l_2) \\ D_{PTLT} = F_D(Z_1, Z_2, \beta l_1, \beta l_2) \end{cases} \quad (6)$$

Based on (5) and (6), Z_1 and Z_2 can be described by βl_1, βl_2, R, X and R_L. (7a) and (7b) could be summarized as follows.

$$\begin{cases} Z_1 = \dfrac{p \cdot q[\cos(\beta l_2) - \cos(\beta l_1)]}{\sin(\beta l_1)[\cos(\beta l_2) + p \cdot X]} \\ Z_2 = \dfrac{p \cdot q[\cos(\beta l_1) - \cos(\beta l_2)]}{\sin(\beta l_2)[\cos(\beta l_1) + p \cdot X]} \end{cases} \quad (7a)$$

or

$$\begin{cases} Z_1 = \dfrac{p \cdot q[\cos(\beta l_1) - \cos(\beta l_2)]}{\sin(\beta l_1)[\cos(\beta l_2) - p \cdot X]} \\ Z_2 = \dfrac{p \cdot q[\cos(\beta l_2) - \cos(\beta l_1)]}{\sin(\beta l_2)[\cos(\beta l_1) - p \cdot X]} \end{cases} \quad (7b)$$

where

$$p = \sqrt{\frac{R_L}{R\left[(R - R_L)^2 + X^2\right]}} \quad (7c)$$

$$q = X^2 + R^2 - R \cdot R_L \quad (7d)$$

B. THE DERIVATION BETWEEN ELECTRICAL LENGTHS AND FREQUENCY RATIO

By analyzing the range of trigonometric function in (7), frequency ratio ranges are determined by l_2/l_1. Because the lengths of two transmission-lines can be selected arbitrary, the general equations can be summarized as

$$\begin{cases} 2a\pi < \beta_1 l_1 < 2(a+1)\pi \\ 2b\pi < \beta_1 l_2 < 2(b+1)\pi \end{cases} \quad (8a)$$

$$\begin{cases} \beta_1 l_1 + \beta_2 l_1 = n\pi \\ \beta_1 l_2 + \beta_2 l_2 = m\pi \end{cases} \quad (8b)$$

where, a, b, m and n are positive integers.

Then, we have $l_2/l_1 = m/n$, the general expression of $\beta_1 l_1$, $\beta_1 l_2$, $\beta_2 l_1$ and $\beta_2 l_2$, can be rewritten as

$$\begin{cases} \beta_1 l_1 = \dfrac{n\pi}{1+u} \\ \beta_1 l_2 = \dfrac{m\pi}{1+u} \end{cases} \quad \text{for frequency } f_1 \quad (9a)$$

$$\begin{cases} \beta_2 l_1 = \dfrac{n\pi}{1+1/u} \\ \beta_2 l_2 = \dfrac{m\pi}{1+1/u} \end{cases} \quad \text{for frequency } f_2 \quad (9b)$$

C. THE CONSTRAINT CONDITIONS OF COMPLEX TERMINAL LOADS FOR DUAL-FREQUENCY OPERATION

The constraint conditions of complex terminal loads (R_1, X_1 and R_2, X_2) for dual-frequency operation is determined by different $(n+m)$. They will be discussed separately.

Firstly, from (7c) and (7d), we have

$$\begin{cases} p_1 = \sqrt{\dfrac{R_L}{R_1\left[(R_1-R_L)^2+X_1^2\right]}} \\ q_1 = X_1^2 + R_1^2 - R_1 \cdot R_L \end{cases} \quad \text{at } f_1 \tag{10a}$$

$$\begin{cases} p_2 = \sqrt{\dfrac{R_L}{R_2\left[(R_2-R_L)^2+X_2^2\right]}} \\ q_2 = X_2^2 + R_2^2 - R_2 \cdot R_L \end{cases} \quad \text{at } f_2 \tag{10b}$$

Then, put (10a) and (10b) into (7a) and (7b), respectively. We have

$$\frac{\pm p_1 \cdot q_1 \left[\cos(\beta_1 l_2) - \cos(\beta_1 l_1)\right]}{\sin(\beta_1 l_1)\left[\cos(\beta_1 l_2) \pm p_1 \cdot X_1\right]} = \frac{\pm p_2 \cdot q_2 \left[\cos(\beta_2 l_2) - \cos(\beta_2 l_1)\right]}{\sin(\beta_2 l_1)\left[\cos(\beta_2 l_2) \pm p_2 \cdot X_2\right]} \tag{11a}$$

$$\frac{\pm p_1 \cdot q_1 \left[\cos(\beta_1 l_1) - \cos(\beta_1 l_2)\right]}{\sin(\beta_1 l_2)\left[\cos(\beta_1 l_1) \pm p_1 \cdot X_1\right]} = \frac{\pm p_2 \cdot q_2 \left[\cos(\beta_2 l_1) - \cos(\beta_2 l_2)\right]}{\sin(\beta_2 l_2)\left[\cos(\beta_2 l_1) \pm p_2 \cdot X_2\right]} \tag{11b}$$

When $(n+m)$ is even integer, the relationship between R_1, X_1 and R_2, X_2 are summarized as

$$\begin{cases} R_2 = R_1 \\ X_2 = -X_1 \end{cases} \tag{12}$$

When $(n+m)$ is odd integer, by using (7a) and (7b), the relationship between R_1, X_1 and R_2, X_2 are summarized as

$$\begin{cases} R_2 = \dfrac{R_L d_2^2}{d_1^2 d_2^2 + R_L^2\left(1-d_1^2\right)^2} \\ X_2 = \dfrac{d_1 d_2\left[d_2^2 - R_L^2\left(1-d_1^2\right)\right]}{d_1^2 d_2^2 + R_L^2\left(1-d_1^2\right)^2} \end{cases} \tag{13a}$$

where

$$\begin{cases} d_1 = \dfrac{p_1 X_1\left[\cos(\beta_1 l_2) - \cos(\beta_1 l_1)\right]}{\pm 2 p_1 X_1 + \left[\cos(\beta_1 l_2) + \cos(\beta_1 l_1)\right]} \\ d_2 = \dfrac{p_1 q_1\left[\cos(\beta_1 l_1) - \cos(\beta_1 l_2)\right]}{\pm 2 p_1 X_1 + \left[\cos(\beta_1 l_2) + \cos(\beta_1 l_1)\right]} \end{cases} \tag{13b}$$

III. THE ANALYSIS OF MAPPING PATTERNS ON EL-EL PLANE

Firstly, the range of R_1, X_1 and R_L must be defined. Based on $Z_1 > 0$, $Z_2 > 0$ and (7), the relationship between designable regions and electrical lengths ratio m/n will be discussed into five different cases in this section, where:

Case I: $R_1 > R_L$

Case II: $R_1 < R_L$ and $X_1^2 < R_1 \cdot R_L - R_1^2$

Case III: $R_1 < R_L$ and $X_1 > \sqrt{R_1 \cdot R_L - R_1^2}$

Case IV: $R_1 < R_L$ and $X_1 < -\sqrt{R_1 \cdot R_L - R_1^2}$

Case V: $R_1 = R_L$

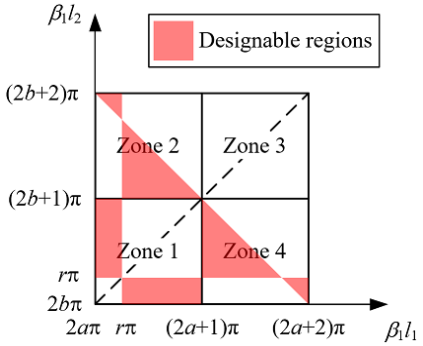

FIGURE 3. The mapping pattern of Case I under the condition of (7a).

A. CASE I

Because $R_1 > R_L$, the design equation (7a) and (7b) should be discussed, respectively.

Firstly, from (7a), Z_1 and Z_2 must be positive value. Then, we have $p_1 > 0$ in (7c), $q_1 > 0$ (7d), $p_1 q_1 > 0$ and $0 < |p_1 X_1| < 1$. The periods of two transmission-lines are 2π, therefore, four zones will be divided and evaluate separately, where, $[2a\pi, 2a\pi+\pi]$ & $[2b\pi, 2b\pi+\pi]$ in Zone 1; $[2a\pi, 2a\pi+\pi]$ & $[2b\pi+\pi, 2b\pi+2\pi]$ in Zone 2; $[2a\pi+\pi, 2a\pi+2\pi]$ & $[2b\pi+\pi, 2b\pi+2\pi]$ in Zone 3; $[2a\pi+\pi, 2a\pi+2\pi]$ & $[2b\pi, 2b\pi+\pi]$ in Zone 4.

In Zone 1, two designable ranges of electrical lengths are

$$\cos(\beta_1 l_2) > \cos(r\pi) > \cos(\beta_1 l_1) \tag{14a}$$

or

$$\cos(\beta_1 l_1) > \cos(r\pi) > \cos(\beta_1 l_2) \tag{14b}$$

where

$$\cos(r\pi) = -p_1 X_1 \tag{14c}$$

From equation (14a), (14b) and (14c), two red rectangle regions are the mapping pattern of Zone 1 in Fig. 3.

In Zone 1, based on (14a) and (14b), we have

$$\begin{cases} (2a+r)\pi < n\pi/(1+u) < (2a+1)\pi \\ 2b\pi < m\pi/(1+u) < (2b+r)\pi \end{cases} \tag{15a}$$

or

$$\begin{cases} 2a\pi < n\pi/(1+u) < (2a+r)\pi \\ (2b+r)\pi < m\pi/(1+u) < (2b+1)\pi \end{cases} \tag{15b}$$

Then, electrical lengths ratios can be derived.

$$2b/(2a+1) < m/n < (2b+r)/(2a+r) \tag{16a}$$

or

$$(2b+r)/(2a+r) < m/n < (2b+1)/2a \tag{16b}$$

The mapping pattern of Zone 1 is also given in Fig. 3, and their frequency ratio ranges are summarized as

$$\left[\frac{n}{2a+1} - 1, \frac{m}{2b+r} - 1\right]_{Max} < u < \left[\frac{n}{2a+r} - 1, \frac{m}{2b} - 1\right]_{Min} \tag{17a}$$

or

$$\left[\frac{n}{2a+r}-1,\frac{m}{2b+1}-1\right]_{Max}<u<\left[\frac{n}{2a}-1,\frac{m}{2b+r}-1\right]_{Min} \quad (17b)$$

By using the similarly discussion above, only the crucial equations are summarized in Zone 2. The relationship of two electrical lengths are

$$\cos(r\pi)>\cos(\beta_1 l_1)>\cos(\beta_1 l_2) \quad (18a)$$

or

$$\cos(\beta_1 l_2)>\cos(\beta_1 l_1)>\cos(r\pi) \quad (18b)$$

Then, the electrical lengths ratios are

$$(2b+1)/(2a+1)<m/n<(2b+2-r)/(2a+r) \quad (18c)$$

or

$$(2b+2-r)/(2a+r)<m/n<(2b+2)/2a \quad (18d)$$

The frequency ratio ranges are

$$\frac{m+n}{2a+2b+2}-1<u<\left[\frac{n}{2a+r}-1,\frac{m}{2b+1}-1\right]_{Min} \quad (18e)$$

or

$$\left[\frac{n}{2a+r}-1,\frac{m}{2b+2}-1\right]_{Max}<u<\frac{m+n}{2a+2b+2}-1 \quad (18f)$$

There is no result in Zone 3. In Zone 4, the relationship of two electrical lengths are

$$\cos(\beta_1 l_1)>\cos(\beta_1 l_2)>\cos(r\pi) \quad (19a)$$

or

$$\cos(r\pi)>\cos(\beta_1 l_2)>\cos(\beta_1 l_1) \quad (19b)$$

The electrical lengths ratios are

$$2b/(2a+2)<m/n<(2b+r)/(2a+2-r) \quad (19c)$$

or

$$(2b+r)/(2a+2-r)<m/n<(2b+1)/(2a+1) \quad (19d)$$

The frequency ratio ranges are

$$\left[\frac{n}{2a+2}-1,\frac{m}{2b+r}-1\right]_{Max}<u<\frac{m+n}{2a+2b+2}-1 \quad (19e)$$

or

$$\frac{m+n}{2a+2b+2}-1<u<\left[\frac{n}{2a+1}-1,\frac{m}{2b+r}-1\right]_{Min} \quad (19f)$$

Finally, under the condition of (7a), the total red designable regions in Fig. 3 are the mapping pattern of Case I.

Secondly, from (7b), Z_1 and Z_2 must be positive value. By using the same process, the detail design equations are listed in Table 2, and the blue designable regions in Fig. 4 are the pattern of Case I.

TABLE 2. For Case I, design equations under the condition of (7b).

Zone 1	The designable ranges of electrical lengths
	None
	The designable ratio of m/n
	None
	The frequency ratio ranges
	None
Zone 2	The designable ranges of electrical lengths
	$\cos(\beta_1 l_2)>\cos(\beta_1 l_1)>-\cos(r\pi)$ or $-\cos(r\pi)>\cos(\beta_1 l_1)>\cos(\beta_1 l_2)$
	The designable ratio of m/n
	$(2b+1)/(2a+1)<m/n<(2b+1+r)/(2a+1-r)$ or $(2b+1+r)/(2a+1-r)<m/n<(2b+2)/2a$
	The frequency ratio ranges
	$\left[\frac{n}{2a+1}-1,\frac{m}{2b+1+r}-1\right]_{Max}<u<\frac{m+n}{2a+2b+2}-1$ or $\frac{m+n}{2a+2b+2}-1<u<\left[\frac{n}{2a}-1,\frac{m}{2b+1+r}-1\right]_{Min}$
Zone 3	The designable ranges of electrical lengths
	$\cos(\beta_1 l_1)>-\cos(r\pi)>\cos(\beta_1 l_2)$ or $\cos(\beta_1 l_2)>-\cos(r\pi)>\cos(\beta_1 l_1)$
	The designable ratio of m/n
	$(2b+1)/(2a+2)<m/n<(2b+1+r)/(2a+1+r)$ or $(2b+1+r)/(2a+1+r)<m/n<(2b+2)/(2a+1)$
	The frequency ratio ranges
	$\left[\frac{n}{2a+2}-1,\frac{m}{2b+1+r}-1\right]_{Max}<u<\left[\frac{n}{2a+1+r}-1,\frac{m}{2b+1}-1\right]_{Min}$ or $\left[\frac{m}{2b+2}-1,\frac{n}{2a+1+r}-1\right]_{Max}<u<\left[\frac{m}{2b+1+r}-1,\frac{n}{2a+1}-1\right]_{Min}$
Zone 4	The designable ranges of electrical lengths
	$-\cos(r\pi)>\cos(\beta_1 l_2)>\cos(\beta_1 l_1)$ or $\cos(\beta_1 l_1)>\cos(\beta_1 l_2)>-\cos(r\pi)$
	The designable ratio of m/n
	$2b/(2a+2)<m/n<(2b+1-r)/(2a+1+r)$ or $(2b+1-r)/(2a+1+r)<m/n<(2b+1)/(2a+1)$
	The frequency ratio ranges
	$\frac{m+n}{2a+2b+2}-1<u<\left[\frac{n}{2a+1+r}-1,\frac{m}{2b}-1\right]_{Min}$ or $\left[\frac{n}{2a+1+r}-1,\frac{m}{2b+1}-1\right]_{Max}<u<\frac{m+n}{2a+2b+2}-1$

B. CASE II

Similarly, the design equation (7a) and (7b) are discussed in Case II, and final design equations are listed in Table 3 (a) and III (b), respectively. The total designable regions in Fig. 5 (a) and (b) are the mapping pattern of Case II.

C. CASE III

Under the conditions of (7a) or (7b), two group of design equations are the same, and they are listed in Table 4,

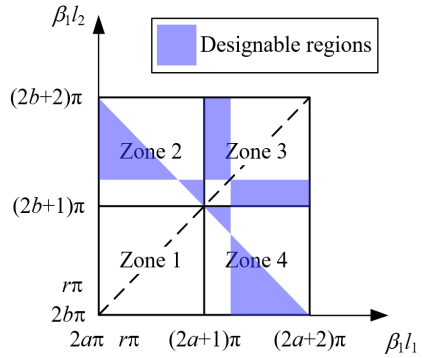

FIGURE 4. The mapping pattern of Case I under the condition of (7b).

therefore, two designable regions are overlapped, and the mapping pattern of Case III are shown in Fig. 6.

D. CASE IV

The design equations are listed in Table 5. Two designable regions are overlapped, and the mapping pattern of Case IV are shown in Fig. 7.

E. CASE V

Because the design equations and designable regions of Case III and IV are exactly the same to those in Case V (when $R_1 = R_L, X_1 > 0$) and (when $R_1 = R_L, X_1 < 0$), respectively. Therefore, these discussions and results are omitted in this paper.

IV. 3D MAPPING APPROACH AND DESIGN EXAMPLES

In order to realize the complex terminal loads Z_S in Fig. 2, two transmission-lines Z_{STL1}, Z_{STL2} and one resistor R_{STL} are cascaded to realize Z_S, where the electrical lengths of Z_{STL1} and Z_{STL2} are θ_{STL1} and θ_{STL2}, respectively. The total topology is shown in Fig. 8.

From Section III, all five cases are introduced in detail, their mapping patterns of designable regions are also drawn on the *EL-EL* plane with design equations. By adding an extra vertical *FR* axis named u, a novel 3D cube can be created on the *FR-EL-EL* coordinate system. For a given electrical lengths ratio $\beta_1 l_2/\beta_1 l_1$, the designable range of frequency ratio can be easily drawn in the 3D cube. Two design examples for Case I and Case III are listed, respectively.

In Example 1, the complex terminal load Z_S is determined as follows: $Z_{S1} = 70 - j50$ @ $f_1 = 1$ GHz and $Z_{S2} = 3.8 - j2.2$ @ $f_2 = 3.6$ GHz, where $u = 3.6$. Because of $R_1 > R_L$, the mapping pattern should belong to Case I. Then, p_1 and r can be calculated from (10a) and (14c), respective. From (14a) and (14b), the mapping pattern of Case I can be easily drawn on the *ADHE* plane in Fig. 9 (a), where, there are two designable regions: red regions and blue regions. When $\beta_1 l_2/\beta_1 l_1 = 1/2$ is given, line *AJ* will through Zone 1 and Zone 4, the *ABIJ* plane can be easily created. If $m = 3$ is fixed, $n = 6$ is automatically determined. By using (9a), the green solid lines can be drawn on the *ABIJ* plane, where, the limitation is determined by (17a) in Zone 1 and (19f) in Zone 4. Finally, two green solid lines are the designable

TABLE 3. (a) For Case II, design equations under the condition of (7a).

Zone 1	The designable ranges of electrical lengths
	None
	The designable ratio of m/n
	None
	The frequency ratio ranges
	None
Zone 2	The designable ranges of electrical lengths
	$\cos(r\pi) > \cos(\beta_1 l_2) > \cos(\beta_1 l_1)$ or $\cos(\beta_1 l_1) > \cos(\beta_1 l_2) > \cos(r\pi)$
	The designable ratio of m/n
	$(2b+1)/(2a+1) < m/n < (2b+2-r)/(2a+r)$ or $(2b+2-r)/(2a+r) < m/n < (2b+2)/2a$
	The frequency ratio ranges
	$\left[\frac{n}{2a+1}-1, \frac{m}{2b+2-r}-1\right]_{Max} < u < \frac{m+n}{2a+2b+2}-1$ or $\frac{m+n}{2a+2b+2}-1 < u < \left[\frac{n}{2a}-1, \frac{m}{2b+2-r}-1\right]_{Min}$
Zone 3	The designable ranges of electrical lengths
	$\cos(\beta_1 l_1) > \cos(r\pi) > \cos(\beta_1 l_2)$ or $\cos(\beta_1 l_2) > \cos(r\pi) > \cos(\beta_1 l_1)$
	The designable ratio of m/n
	$(2b+1)/(2a+2) < m/n < (2b+2-r)/(2a+2-r)$ or $(2b+2-r)/(2a+2-r) < m/n < (2b+2)/(2a+1)$
	The frequency ratio ranges
	$\left[\frac{n}{2a+2}-1, \frac{m}{2b+2-r}-1\right]_{Max} < u < \left[\frac{n}{2a+2-r}-1, \frac{m}{2b+1}-1\right]_{Min}$ or $\left[\frac{n}{2a+2-r}-1, \frac{m}{2b+2}-1\right]_{Max} < u < \left[\frac{n}{2a+1}-1, \frac{m}{2b+2-r}-1\right]_{Min}$
Zone 4	The designable ranges of electrical lengths
	$\cos(\beta_1 l_2) > \cos(\beta_1 l_1) > \cos(r\pi)$ or $\cos(r\pi) > \cos(\beta_1 l_1) > \cos(\beta_1 l_2)$
	The designable ratio of m/n
	$2b/(2a+2) < m/n < (2b+r)/(2a+2-r)$ or $(2b+r)/(2a+2-r) < m/n < (2b+1)/(2a+1)$
	The frequency ratio ranges
	$\frac{m+n}{2a+2b+2}-1 < u < \left[\frac{n}{2a+2-r}-1, \frac{m}{2b}-1\right]_{Min}$ or $\left[\frac{n}{2a+2-r}-1, \frac{m}{2b+1}-1\right]_{Max} < u < \frac{m+n}{2a+2b+2}-1$

frequency ratio ranges of proposed topology. By the way, two black solid lines which on the *ABFE* plane and *ABCD* plane are the projection of the green solid lines. Corresponding to Fig. 9 (a), the detail design parameters of Example 1 are also listed in Table 6, and its circuit simulation result is shown in Fig. 10 (a), where, the characteristic impedances and their electrical lengths are calculated from (7b) and (9a), respectively.

TABLE 3. *(Continued.)* **(b) For Case II, design equations under the condition of (7b).**

Zone 1	The designable ranges of electrical lengths
	$\cos(\beta_1 l_1) > -\cos(r\pi) > \cos(\beta_1 l_2)$ or $\cos(\beta_1 l_2) > -\cos(r\pi) > \cos(\beta_1 l_1)$
	The designable ratio of m/n
	$2b/(2a+1) < m/n < (2b+1-r)/(2a+1-r)$ or $(2b+1-r)/(2a+1-r) < m/n < (2b+1)/2a$
	The frequency ratio ranges
	$\left[\frac{n}{2a+1}-1, \frac{m}{2b+1-r}-1\right]_{Max} < u < \left[\frac{n}{2a+1-r}-1, \frac{m}{2b}-1\right]_{Min}$ or $\left[\frac{n}{2a+1-r}-1, \frac{m}{2b+1}-1\right]_{Max} < u < \left[\frac{n}{2a}-1, \frac{m}{2b+1-r}-1\right]_{Min}$
Zone 2	The designable ranges of electrical lengths
	$-\cos(r\pi) > \cos(\beta_1 l_1) > \cos(\beta_1 l_2)$ or $\cos(\beta_1 l_2) > \cos(\beta_1 l_1) > -\cos(r\pi)$
	The designable ratio of m/n
	$(2b+1)/(2a+1) < m/n < (2b+1+r)/(2a+1-r)$ or
	$(2b+1+r)/(2a+1-r) < m/n < (2b+2)/2a$
	The frequency ratio ranges
	$\frac{m+n}{2a+2b+2}-1 < u < \left[\frac{n}{2a+1-r}-1, \frac{m}{2b+1}-1\right]_{Min}$ or $\left[\frac{n}{2a+1-r}-1, \frac{m}{2b+2}-1\right]_{Max} < u < \frac{m+n}{2a+2b+2}-1$
Zone 3	The designable ranges of electrical lengths
	None
	The designable ratio of m/n
	None
	The frequency ratio ranges
	None
Zone 4	The designable ranges of electrical lengths
	$\cos(\beta_1 l_1) > \cos(\beta_1 l_2) > -\cos(r\pi)$ or $-\cos(r\pi) > \cos(\beta_1 l_2) > \cos(\beta_1 l_1)$
	The designable ratio of m/n
	$2b/(2a+2) < m/n < (2b+1-r)/(2a+1+r)$ or $(2b+1-r)/(2a+1+r) < m/n < (2b+1)/(2a+1)$
	The frequency ratio ranges
	$\left[\frac{n}{2a+2}-1, \frac{m}{2b+1-r}-1\right]_{Max} < u < \frac{m+n}{2a+2b+2}-1$ or $\frac{m+n}{2a+2b+2}-1 < u < \left[\frac{n}{2a+1}-1, \frac{m}{2b+1-r}-1\right]_{Min}$

For Example 1, the design parameters are shown in Table 6, Rogers RT/6010 substrate is used for demonstration. The data of the substrate are $\varepsilon_r = 10.2$, $\tan\delta = 0.0023$, thickness of dielectric layer $h = 1.27$ mm, and conductor thickness $t = 0.018$ mm. Fig. 11 shows the fabricated circuit and its simulated and experimental results.

Similarly, for Case III, Example 2 is also discussed in this section, the parameters of complex terminal load are:

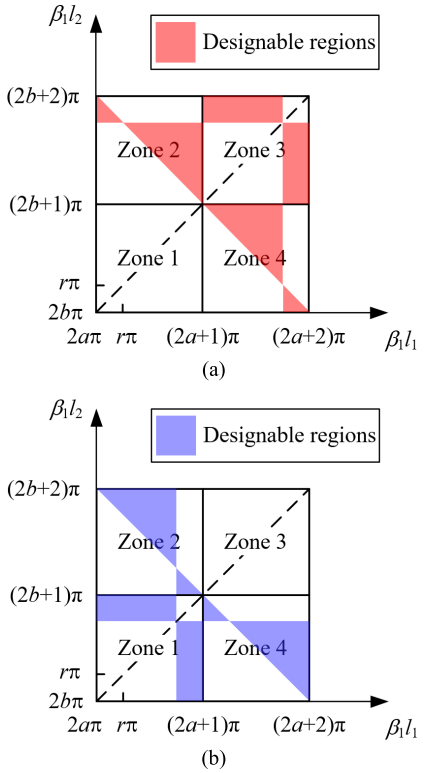

FIGURE 5. The mapping pattern of Case II. (a) The mapping pattern under the condition of (7a). (b) The mapping pattern under the condition of (7b).

TABLE 4. For Case III, design equations under the condition of (7a) or (7b).

Zone 1	The designable ranges of electrical lengths
	None
	The designable ratio of m/n
	None
	The frequency ratio ranges
	None
Zone 2	The designable ranges of electrical lengths
	$\cos(\beta_1 l_1) > \cos(\beta_1 l_2)$
	The designable ratio of m/n
	$(2b+1)/(2a+1) < m/n < (2b+2)/2a$
	The frequency ratio ranges
	$\frac{m+n}{2a+2b+2}-1 < u < \left[\frac{n}{2a}-1, \frac{m}{2b+1}-1\right]_{Min}$
Zone 3	The designable ranges of electrical lengths
	None
	The designable ratio of m/n
	None
	The frequency ratio ranges
	None
Zone 4	The designable ranges of electrical lengths
	$\cos(\beta_1 l_2) > \cos(\beta_1 l_1)$
	The designable ratio of m/n
	$2b/(2a+2) < m/n < (2b+1)/(2a+1)$
	The frequency ratio ranges
	$\frac{m+n}{2a+2b+2}-1 < u < \left[\frac{n}{2a+1}-1, \frac{m}{2b}-1\right]_{Min}$

$Z_{S1} = 40 - j200$ @ $f_1 = 1$ GHz and $Z_{S2} = 40 + j200$ @ $f_2 = 2.2$ GHz. Its 3D designable frequency ratio

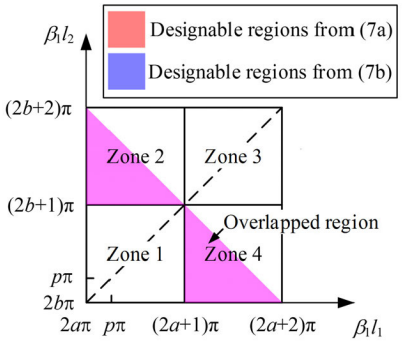

FIGURE 6. The mapping pattern of Case III.

TABLE 5. For Case IV, design equations under the condition of (7a) or (7b).

Zone 1	The designable ranges of electrical lengths
	None
	The designable ratio of m/n
	None
	The frequency ratio ranges
	None
Zone 2	The designable ranges of electrical lengths
	$\cos(\beta_1 l_2) > \cos(\beta_1 l_1)$
	The designable ratio of m/n
	$(2b+1)/(2a+1) < m/n < (2b+2)/2a$
	The frequency ratio ranges
	$\left[\frac{n}{2a+1}-1, \frac{m}{2b+2}-1\right]_{Max} < u < \frac{m+n}{2a+2b+2}-1$
Zone 3	The designable ranges of electrical lengths
	The designable ratio of m/n
	None
	The frequency ratio ranges
	None
	The designable ratio of m/n
Zone 4	The designable ranges of electrical lengths
	$\cos(\beta_1 l_1) > \cos(\beta_1 l_2)$
	The designable ratio of m/n
	$2b/(2a+2) < m/n < (2b+1)/(2a+1)$
	The frequency ratio ranges
	$\left[\frac{n}{2a+2}-1, \frac{m}{2b+1}-1\right]_{Max} < u < \frac{m+n}{2a+2b+2}-1$

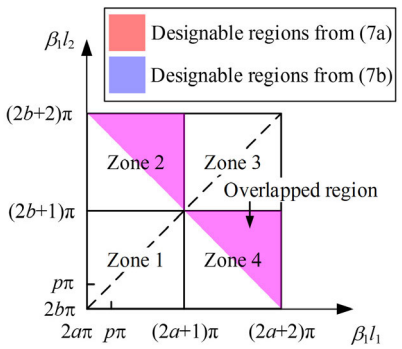

FIGURE 7. The mapping pattern of Case IV.

ranges are shown in Fig. 9(b). Detail design parameters are listed in Table 6, and its circuit simulation result is shown in Fig. 10 (b).

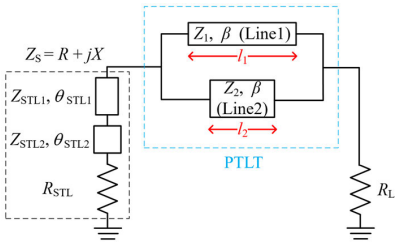

FIGURE 8. The topology of proposed dual-frequency PTLT with complex terminal load.

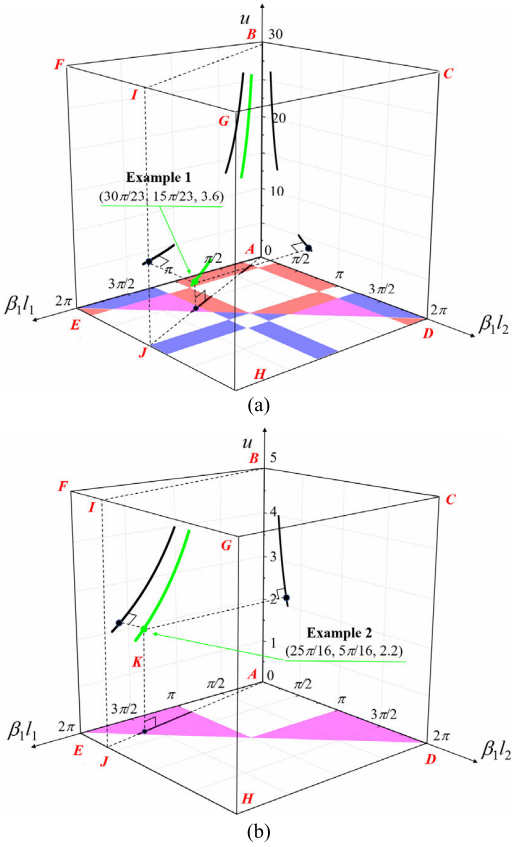

FIGURE 9. Two design examples on the 3D *FR-EL-EL* coordinate. (a) Design example in Case I, where $r = 0.21$. (b) Design example in Case III.

TABLE 6. Design parameters of dual-frequency parallel transmission-line transformer, where $R_L = 50\ \Omega$.

The 3D positions of design example	Terminal load Z_S		Design parameters of PTLT
Example 1 $\left(\frac{30}{23}\pi, \frac{15}{23}\pi, 3.6\right)$	$Z_{STL1} = 16.4\ \Omega$, $\theta_{STL1} = 18.3°@f_1$ $Z_{STL2} = 68.9\ \Omega$, $\theta_{STL2} = 41.8°@f_1$ $R_{STL} = 23.6\ \Omega$.	Z_{S1}=70-*j*50 @f_1 Z_{S2}=3.8-*j*2.2 @f_2	$Z_1 = 26.9\ \Omega$, $\theta_1 = 234.8°@f_1$ $Z_2 = 38.6\ \Omega$, $\theta_2 = 117.4°@f_1$ $u = f_2/f_1 = 3.6$.
Example 2 $\left(\frac{25}{16}\pi, \frac{5}{16}\pi, 2.2\right)$	$Z_{STL1} = 80.3\ \Omega$, $\theta_{STL1} = 56.3°@f_1$ $Z_{STL2} = 76.5\ \Omega$, $\theta_{STL2} = 56.3°@f_1$ $R_{STL} = 5.0\ \Omega$.	Z_{S1}=40-*j*200 @f_1 Z_{S2}=40+*j*200 @f_2	$Z_1 = 144.8\ \Omega$, $\theta_1 = 281.3°@f_1$ $Z_2 = 104.0\ \Omega$, $\theta_2 = 56.3°@f_1$ $u = f_2/f_1 = 2.2$.

V. EXPERIMENT

Corresponding to Example 1 and 2, two experimental circuits were fabricated, simulated and measured, respectively.

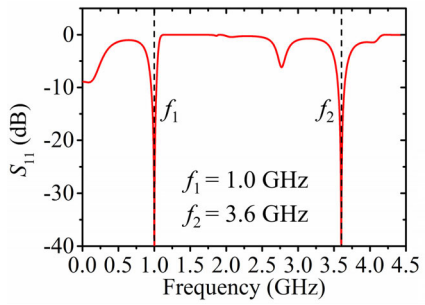

(a)

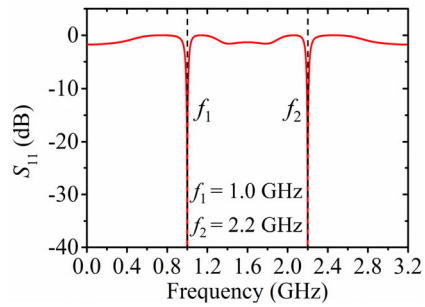

(b)

FIGURE 10. Ideal frequency characteristics for two design examples of dual-frequency PTLT (corresponding to Table 6). (a) Example 1. (b) Example 2.

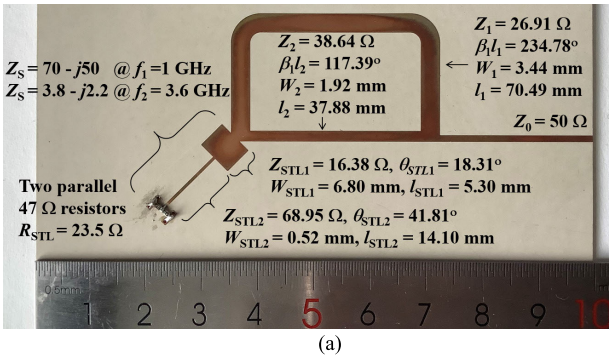

(a)

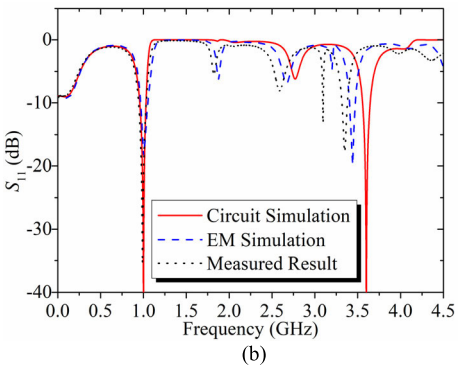

(b)

FIGURE 11. Experimental results of Example 1. (a) Fabricated circuit. (b) Circuit simulation, EM simulation and measured results.

EM simulated and measured results are matched very well.

For Example 2, the design parameters are also shown in Table 6, NPC-F260A substrate is used for demonstration.

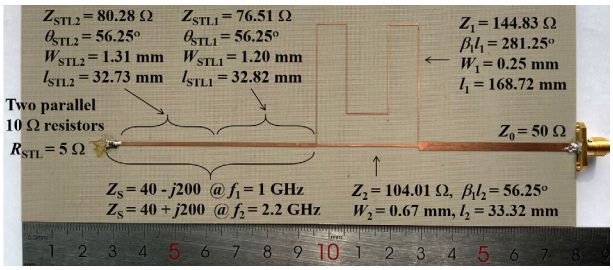

(a)

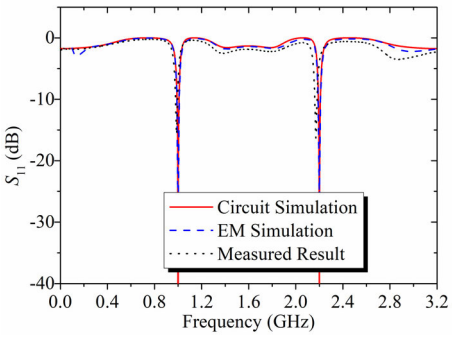

(b)

FIGURE 12. Experimental results of Example 2. (a) Fabricated circuit. (b) Circuit simulation, EM simulation and measured results.

The data of the substrate are $\varepsilon_r = 2.6$, $\tan\delta = 0.004$, thickness of dielectric layer $h = 0.996$ mm, and conductor thickness $t = 0.018$ mm. Fig. 12 shows the fabricated circuit and its simulated and experimental results.

VI. CONCLUSION

In this paper, a parallel transmission-line transformer with complex terminal loads was introduced for dual-frequency design. Four different mapping patterns of designable regions were newly summarized on the *EL-EL* plane under the conditions of different cases of complex terminal loads. By adding an extra vertical *FR* axis, the designable ranges of frequency ratio could be easily drawn in the 3D cube on the *FR-EL-EL* coordinate system. The visible 3D mapping approach matched the complex terminal load of parallel transmission-line transformer at two different frequencies. For the certain pattern, clearly boundary distinguished the designable and undesignable ranges. For verification, two examples were designed, fabricated and measured. Simulated and measured results were matched very well.

REFERENCES

[1] H.-R. Ahn, "Complex impedance transformers consisting of only transmission-line sections," *IEEE Trans. Microw. Theory Techn.*, vol. 60, no. 7, pp. 2073–2084, Jul. 2012.

[2] Y. L. Chow and K. L. Wan, "A transformer of one-third wavelength in two sections—For a frequency and its first harmonic," *IEEE Microw. Wireless Compon. Lett.*, vol. 12, no. 1, pp. 22–23, Jan. 2002.

[3] C. Monzon, "Analytical derivation of a two-section impedance transformer for a frequency and its first harmonic," *IEEE Microw. Wireless Compon. Lett.*, vol. 12, no. 10, pp. 381–382, Oct. 2002.

[4] C. Monzon, "A small dual-frequency transformer in two sections," *IEEE Trans. Microw. Theory Techn.*, vol. 51, no. 4, pp. 1157–1161, Apr. 2003.

[5] S. J. Orfanidis, "A two-section dual-band Chebyshev impedance transformer," *IEEE Microw. Wireless Compon. Lett.*, vol. 13, no. 9, pp. 382–384, Sep. 2003.
[6] R. Darraji, M. M. Honari, R. Mirzavand, F. M. Ghannouchi, and P. Mousavi, "Wideband two-section impedance transformer with flat real-to-real impedance matching," *IEEE Microw. Wireless Compon. Lett.*, vol. 26, no. 5, pp. 313–315, May 2016.
[7] M. Chongcheawchamnan, S. Patisang, S. Srisathit, R. Phromloungsri, and S. Bunnjaweht, "Analysis and design of a three-section transmission-line transformer," *IEEE Trans. Microw. Theory Techn.*, vol. 53, no. 7, pp. 2458–2462, Jul. 2005.
[8] L. Liu, J. Geng, F. Liu, H. Fan, X. Liang, W. Wang, and R. Jin, "A novel analytical method for multi-frequency transmission line transformer," *IEEE Microw. Wireless Compon. Lett.*, vol. 26, no. 8, pp. 556–558, Aug. 2016.
[9] L. Liu, R. Jin, X. Liang, H. Fan, W. Wang, J. Geng, F. Liu, and Y. Chen, "Multifrequency transformer with arbitrary frequency and real impedance transform ratio," *IEEE Microw. Wireless Compon. Lett.*, vol. 27, no. 9, pp. 785–787, Sep. 2017.
[10] Y. Wu, Y. Liu, and S. Li, "A dual-frequency transformer for complex impedances with two unequal sections," *IEEE Microw. Wireless Compon. Lett.*, vol. 19, no. 2, pp. 77–79, Feb. 2009.
[11] X. Liu, Y. Liu, S. Li, F. Wu, and Y. Wu, "A three-section dual-band transformer for frequency-dependent complex load impedance," *IEEE Microw. Wireless Compon. Lett.*, vol. 19, no. 10, pp. 611–613, Oct. 2009.
[12] Y. Wu, Y. Liu, S. Li, C. Yu, and X. Liu, "A generalized dual-frequency transformer for two arbitrary complex frequency-dependent impedances," *IEEE Microw. Wireless Compon. Lett.*, vol. 19, no. 12, pp. 792–794, Dec. 2009.
[13] T. Jensen, V. Zhurbenko, V. Krozer, and P. Meincke, "Coupled transmission lines as impedance transformer," *IEEE Trans. Microw. Theory Techn.*, vol. 55, no. 12, pp. 2957–2965, Dec. 2007.
[14] H.-R. Ahn and T. Itoh, "Impedance-transforming symmetric and asymmetric DC blocks," *IEEE Trans. Microw. Theory Techn.*, vol. 58, no. 9, pp. 2463–2474, Sep. 2010.
[15] H. T. Nguyen, K. S. Ang, and G. I. Ng, "Design of coupled three-line impedance transformers," *IEEE Microw. Wireless Compon. Lett.*, vol. 24, no. 2, pp. 84–86, Feb. 2014.
[16] Y.-F. Bai, X.-H. Wang, C.-J. Gao, Q.-L. Huang, and X.-W. Shi, "Design of compact quad-frequency impedance transformer using two-section coupled line," *IEEE Trans. Microw. Theory Techn.*, vol. 60, no. 8, pp. 2417–2423, Aug. 2012.
[17] N.-C. Kuo, C.-N. Chiu, H.-C. Hsieh, and J.-S. Chen, "Radiation minimization of single-stub microstrip impedance transformers," *IEEE Trans. Microw. Theory Techn.*, vol. 61, no. 3, pp. 1018–1029, Mar. 2013.
[18] M.-L. Chuang, "Dual-band impedance transformer using two-section shunt stubs," *IEEE Trans. Microw. Theory Techn.*, vol. 58, no. 5, pp. 1257–1263, May 2010.
[19] O. Manoochehri, A. Asoodeh, and K. Forooraghi, "Π-model dual-band impedance transformer for unequal complex impedance loads," *IEEE Microw. Wireless Compon. Lett.*, vol. 25, no. 4, pp. 238–240, Apr. 2015.
[20] M.-L. Chuang and M.-T. Wu, "Transmission zero embedded dual-band impedance transformer with three shunt stubs," *IEEE Microw. Wireless Compon. Lett.*, vol. 27, no. 9, pp. 788–790, Sep. 2017.
[21] Y. Liu, Y. Zhao, S. Liu, Y. Zhou, and Y. Chen, "Multi-frequency impedance transformers for frequency-dependent complex loads," *IEEE Trans. Microw. Theory Techn.*, vol. 61, no. 9, pp. 3225–3235, Sep. 2013.
[22] P. Kim, G. Chaudhary, and Y. Jeong, "Ultra-high transforming ratio coupled line impedance transformer with bandpass response," *IEEE Microw. Wireless Compon. Lett.*, vol. 25, no. 7, pp. 445–447, Jul. 2015.
[23] R. Zhang, S. Luo, and L. Zhu, "Synthesis and design of mixed lumped and distributed low-pass filters/low-passing impedance transformers with Taylor series," *IEEE Trans. Microw. Theory Techn.*, vol. 64, no. 4, pp. 1265–1272, Apr. 2016.
[24] Q.-S. Wu and L. Zhu, "Wideband impedance transformers with good frequency selectivity based on multisection quarter-wave lines and short-circuited stubs," *IEEE Microw. Wireless Compon. Lett.*, vol. 26, no. 5, pp. 337–339, May 2016.
[25] Q.-S. Wu and L. Zhu, "Short-ended coupled-line impedance transformers with ultrahigh transforming ratio and bandpass selectivity suitable for large load impedances," *IEEE Trans. Compon., Packag., Manuf. Technol.*, vol. 6, no. 5, pp. 767–774, May 2016.
[26] Y. Liu, "Synthesis techniques on multiband impedance matching networks for frequency-dependent complex loads," *IEEE Trans. Microw. Theory Techn.*, vol. 66, no. 10, pp. 4507–4519, Oct. 2018.
[27] R. Sinha and A. De, "Theory on matching network in viewpoint of transmission phase shift," *IEEE Trans. Microw. Theory Techn.*, vol. 64, no. 6, pp. 1704–1716, Jun. 2016.
[28] R. Gómez-García and J. I. Alonso, "Design of sharp-rejection and low-loss wide-band planar filters using signal-interference techniques," *IEEE Microw. Wireless Compon. Lett.*, vol. 15, no. 8, pp. 530–532, Aug. 2005.
[29] R. Gómez-García, M. Sánchez-Renedo, B. Jarry, J. Lintignat, and B. Barelaud, "A class of microwave transversal signal-interference dual-passband planar filters," *IEEE Microw. Wireless Compon. Lett.*, vol. 19, no. 3, pp. 158–160, Mar. 2009.
[30] R. Gómez-García, J.-M. Muñoz-Ferreras, and M. Sanchez-Renedo, "Signal-interference stepped-impedance-line microstrip filters and application to duplexers," *IEEE Microw. Wireless Compon. Lett.*, vol. 21, no. 8, pp. 421–423, Aug. 2011.
[31] X. Wang, Z. Ma, and M. Ohira, "Dual-band design theory for dual transmission-line transformer," *IEEE Microw. Wireless Compon. Lett.*, vol. 27, no. 9, pp. 782–784, Sep. 2017.
[32] R. Sinha and H. Son, "Comments on dual-band design theory for dual transmission-line transformer," *IEEE Microw. Wireless Compon. Lett.*, vol. 28, no. 12, pp. 1155–1157, Dec. 2018.
[33] X. Wang, T. Xie, G. Lu, Z. Ma, and M. Ohira, "Authors' reply," *IEEE Microw. Compon. Lett.*, vol. 28, no. 12, pp. 1158–1159, Dec. 2018.

TAIYANG XIE was born in Liaoyuan, China, in 1994. He received the B.S. degree from the College of Electronic Science and Engineering, Jilin University, Changchun, China, in 2017, where he is currently pursuing the M.S. degree.

His research interests included analysis and design of ultrawideband bandpass filtering circuits and dual-frequency transmission-line circuit.

XIAOLONG WANG (Member, IEEE) received the B.S. degree in communication engineering from Jilin University, Changchun, China, in 2005, the M.S. degree from the Changchun University of Science and Technology, Changchun, in 2008, and the Ph.D. degree from the University of Toyama, Toyama, Japan, in 2012. From November 2012 to June 2013, he was a Postdoctoral Research Associate with the Art, Science and Technology Center for Cooperative Research, Kyushu University, Japan. From July 2013 to December 2015, he was a Researcher with the Plasma Research Center, University of Tsukuba, Japan. Since January 2016, he has been an Assistant Professor with the Department of Electronic Engineering, Saitama University, Japan. He is currently a Professor with the College of Electronic Science and Engineering, Jilin University, China. His research interests include microwave/millimeter-wave system design, passive component design, and optimization techniques.

Dr. Wang is a member of the Institute of Electronics, Information and Communication Engineers (IEICE), Japan. He was a recipient of the IEEE MTT-S Japan Chapter Young Engineer Award, in 2013.

ZHEWANG MA (Member, IEEE) received the B.Eng. and M.Eng. degrees from the University of Science and Technology of China (USTC), Hefei, China, in 1986 and 1989, respectively, and the Dr.Eng. degree from the University of Electro-Communications, Tokyo, Japan, in 1995.

From 1985 to 1989, he was engaged in research works on dielectric waveguides, resonators, and leaky-wave antennas. He was a Research Assistant with the Department of Electronic Engineering, The University of Electro-Communications, in 1996, where he became an Associate Professor, in 1997. From 1990 to 1997, he did studies on computational electromagnetics, analytical and numerical modeling of various microwave, and millimeter wave transmission lines and circuits. From 1998 to 2008, he was an Associate Professor with the Department of Electrical and Electronic Systems, Saitama University, Japan, where he was promoted to a Professor, in 2009. His current research works are mainly on the development of microwave and millimeter-wave devices and circuits, measurements of dielectric materials, and high-temperature superconductors.

Mr. Ma was a Research Fellow of the Japan Society for the Promotion of Science (JSPS), from 1994 to 1996. He was a member of the Steering and/or Technical Committee of the Asia Pacific Microwave Conference. He is a Senior Member of the Institute of Electronics, Information and Communication Engineers (IEICE) of Japan. He received the Japanese Government Graduate Scholarship, from 1991 to 1993. He was granted the URSI Young Scientist Award, in 1993. He was awarded the CJMW Microwave Prize, in 2008 and 2011. He was also a recipient of the Best Paper Award from IEICE, in 2018. He is the Vice-President of the Technical Group on Electronics Simulation Technology of the Electronics Society, IEICE. He has served on the Editorial Board of the IEEE TRANSACTIONS ON MICROWAVE THEORY AND TECHNIQUES, Review Board of the IEEE MICROWAVE AND WIRELESS COMPONENTS LETTERS, Review Board of the *International Journal of RF and Microwave Computer-Aided Engineering*, Review Board of *IEICE Transactions on Electronics*, Japan, and as an Editor of two Special Issues of *IEICE Transactions on Electronics*.

CHUN-PING CHEN (Member, IEEE) received the B.Eng. and Dr.Eng. degrees in microwave and electromagnetic field engineering from Shanghai University, Shanghai, China, in 1999 and 2004, respectively. From 2004 to 2006, he was continuing his research as a Visiting Researcher with Kanagawa University, Japan. Since 2006, he has been a Research Assistant with the Department of Electronic, Electronics and Information Engineering, Kanagawa University. In 2009, he became an Assistant Professor and in 2017, he was promoted to an Associate Professor at Kanagawa University. His research interests include microwave planar circuit design, materials' EM-property measurement, and EMC related techniques. He is a member of IEICE. He received the Young Researcher's Award of IEICE, in 2009. He has served on the Editorial Board of the IEEE TRANSACTIONS ON MICROWAVE THEORY AND TECHNIQUES, Review Board of the IEEE MICROWAVE AND WIRELESS COMPONENTS LETTERS, Review Board of *IET Microwaves, Antennas and Propagation*, and Review Board of *IEICE Transactions on Electronics*, and an Associate Editor of *IEICE Electronics Express*, Japan. He is also serving as a Committee Member for the IEEE Microwave Theory and Techniques Society Japan Chapter.

GEYU LU received the B.Sc. degree in electronic sciences and the M.S. degree from Jilin University, China, in 1985 and 1988, respectively, and the Dr.Eng. degree from Kyushu University, Japan, in 1998. He is currently a Professor with Jilin University. His current research interests include the development of chemical sensors and the application of the function materials.